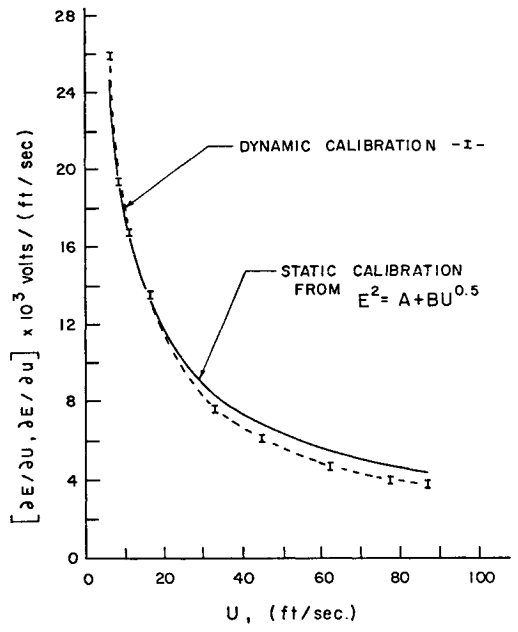

Fig. 2 Linear response terms.

tested, the difference between the static and the dynamic calibration can be as large as 15%. There is no choice of exponent n in King's Law which will produce agreement between the static and dynamic calibration over this range of mean flow velocity.

The measurement of absolute turbulent intensity using the dynamic calibration suggested herein is believed to be more accurate than the static calibration, because the dynamic calibration more correctly models the mode of heat transfer between the wire and the turbulent flow. There are some data in Ref. 4 to support this conclusion.

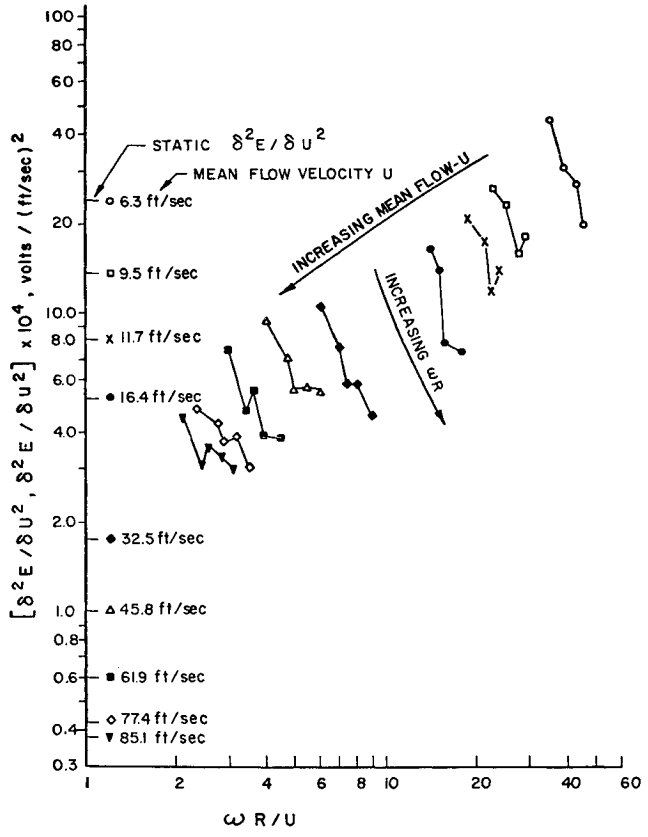

Fig. 3 Second-order response.

Figure 3 is a plot of $\partial^2 E/\partial U^2$ from the static calibration and $\partial^2 E/\partial u^2$ from the coefficient of $\cos 2\omega t$ in Eq. (1) vs the parameter $(\omega R/U)$. The striking feature of these data is the strong dependence of $\partial^2 E/\partial u^2$ on the artificial turbulence level $\omega R/U$. This dependence is not predicted from the second derivative of the static calibration curve $E^2 = A + BU^n$ nor is it observed in the first term of the dynamic response $\partial E/\partial u$. These data indicate that the nonlinear part of the wire response in Eq. (4) is frequency dependent over the range investigated in this experiment. At the higher mean flows, there is considerable discrepancy between the static $\partial^2 E/\partial U^2$ and the dynamic $\partial^2 E/\partial u^2$. Both of these facts contribute to uncertainties in the determination of absolute turbulent intensity.

Conclusions

A technique has been presented which provides for the direct calibration of a hot wire anemometer for turbulence intensity measurements without recourse to the static King's Law response curve. The linear part of the response curve is in agreement with the data of previous workers.[4] The nonlinear part of the response has been found to be dependent on the frequency of the artificial turbulence used to calibrate the probe, indicating that turbulent intensity, as determined from Eq. (4), is a function of its spectral distribution.

Further work is presently underway to determine the bridge voltage response to both longitudinal and transverse velocity perturbations represented by an expansion of $E(U+u, v)$.

References

[1] Bradshaw, P., *An Introduction to Turbulence and its Measurement*, Pergamon Press, New York, 1971.

[2] Hinze, J. O., *Turbulence, An Introduction to its Mechanism and Theory*, McGraw-Hill, New York, 1959.

[3] Vernotte, P., "L'anemometrie des courants turbulents par le fil chaud," *Comptes Rendus*, Vol. 230, 1950, p. 58.

[4] Perry, A. E. and Morrison, G. L., "Static and Dynamic Calibrations of Constant Temperature Hot Wire Systems," *Journal of Fluid Mechanics*, Vol. 47, 1971, pp. 765–773.

[5] Fisher, J. C., "Lock in the Devil, Educe Him, or Take Him for the Last Ride in a Boxcar," *P.A.R. Research Note*, Vol. 6, No. 1, 1960.

[6] Wilson, E. B., *An Introduction to Scientific Research*, McGraw-Hill, New York, 1952, pp. 102–104.

[7] Gorman, D. J., private communication, Dept. of Mechanical Engineering, Univ. of Ottawa, Ontario, Canada.

Turbulence Measurements in a Mach 2.9 Boundary Layer Using Laser Velocimetry

DENNIS A. JOHNSON*
NASA Ames Research Center, Moffett Field, Calif.

Nomenclature

d_f = distance between interference fringes
d_p = diameter of particle
f_{3db} = frequency related to particle response—3 db point
k = Cunningham constant, 1.8 for air

Received July 2, 1973; revision received October 18, 1973.
Index categories: Boundary Layers and Convective Heat Transfer—Turbulent; Supersonic and Hypersonic Flows; Research Facilities and Instrumentation.

* NRC Postdoctoral Research Associate. Associate Member AIAA.

l = mean free path
t_f = time between fringe crossings
u = velocity component parallel to freestream velocity
u_c = convection velocity
u_τ = shear velocity
v = velocity component normal to upper wind-tunnel wall
V = velocity component normal to interference fringes
w = transverse velocity component
y = distance from upper wind-tunnel wall
δ = boundary-layer thickness
θ = angle between incident laser beams
λ_0 = wavelength of laser light
μ = molecular viscosity
ρ = fluid density
ρ_p = particle density
$\langle\ \rangle$ = standard deviation of bracketed quantity

Superscripts

$(\ )'$ = fluctuation quantity, time-averaged value of zero
$\bar{(\ )}$ = time-averaged quantity

Subscripts

w = wall value
∞ = freestream value

I. Introduction

THE nonperturbing characteristic, sole velocity sensitivity, and instantaneous velocity capability of the laser velocimeter make it very attractive as a measurement tool to determine in detail the characteristics of subsonic, transonic, and supersonic flows. However, the underlying question in applying a laser velocimeter to these flows (especially in the transonic and supersonic cases) is whether it can determine accurately the velocities of particles sufficiently small that particle slippage is negligible. In this Note, laser velocimeter measurements employing single-particle, time-domain signal processing, of a Mach 2.9 wind-tunnel-wall turbulent boundary layer are presented which support an affirmative answer to this question.

Quantities measured include the streamwise mean velocity (which is compared to pitot tube data), the turbulence intensity in the streamwise direction, and the velocity correlation, $\overline{u'v'}$. It is the product of this latter quantity and the local fluid density, $\bar{\rho}\overline{u'v'}$, which is generally consider to represent the Reynolds shear stress for compressible boundary-layer flows.[1-3] The measurements presented here should be taken as preliminary. However, more extensive LDV measurements are currently being obtained and compared with hot-wire anemometer data taken at the same time, under the same flow conditions in the Ames Research Center supersonic tunnel; these data will be reported in the near future.

II. Experiment

The study was conducted in the Ames 20.32 cm by 20.32 cm supersonic blowdown wind tunnel. Test conditions were a freestream Mach number of 2.9, a stagnation pressure and temperature of 6.8 atm and 291°K, respectively, and a freestream unit Reynolds number of 5.7×10^7/m.

The region of interest was the turbulent boundary layer on the nearly adiabatic upper nozzle wall of which a detailed flowfield survey (pitot and static pressure) had previously been made by Reda and Murphy.[4] All the laser velocimeter measurements were made at one test section location at which these data were available. At this station and at least 10 boundary-layer thicknesses upstream, the pressure gradient was essentially zero.

A schematic representation of the laser velocimeter system employed and its relation to the wind-tunnel test section is shown in Fig. 1. The optical arrangement was of the standard "dual scatter" or "fringe mode" type. With this configuration, the velocity component sensed lies in the plane formed by the two incident laser beams and is perpendicular to their bisector. Thus, by simply rotating the splitter cube, various sensitivities to u and v with the attendant insensitivity to the w component can be obtained. This capability was utilized to determine the velocity

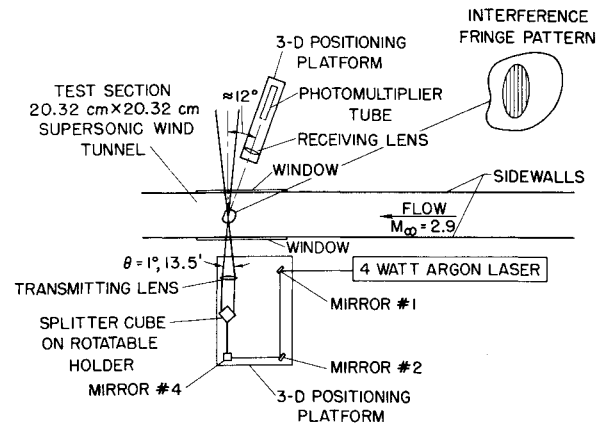

Fig. 1 Schematic representation of laser velocimeter optical arrangement.

correlation, $\overline{u'v'}$, by taking measurements with the laser beams orientated at $+45°$ and $-45°$ with respect to the streamwise direction (in a manner analogous to the slanted hot-wire technique and as applied in other laser velocimeter investigations[5,6]).

The angle formed by the two incident beams, θ (which must be known to establish the fringe spacing, $d_f = \lambda_0/2\sin(\theta/2)$, and consequently, the velocity, $V = d_f/t_f$), was determined to within an estimated accuracy of $\pm\frac{1}{2}\%$ by measuring the separation of the laser beams at a distance close to 4 m from the beam crossover point. The beam separation was established by a transverse scan with a photomultiplier tube masked by a 0.25-mm-diam pinhole. From oscilloscope displays of the single-particle signals, the laser beam diameter ($1/e^2$) at the beam crossover point, which determines the effective spatial resolution of the laser velocimeter, was estimated to be 300 μm.

The time between fringe crossings (i.e., the time between zero crossings of the signals bursts after pedestal removal) was measured with an AEDC laser Doppler processing unit.[7] Data reduction was accomplished by coupling the processing unit to a programable calculator. The calculator was programed to compute the mean velocity and turbulence intensity based on 100 measurements by the following statistics:

$$\bar{V} = \frac{\sum_{i=1}^{100} V_i}{100}; \quad \frac{\langle V' \rangle}{\bar{V}} = \frac{\left(\sum_{i=1}^{100} \frac{V_i^2}{100} - \bar{V}^2\right)^{1/2}}{\bar{V}}$$

and to recalculate these quantities based on the next 100 measurements which satisfied the condition

$$|V_i - \bar{V}_1| \leqq 3\langle V_1' \rangle$$

where subscript 1 denotes the quantities determined from the first sample. This test of the data was employed to minimize the effects of spurious measurments on the data caused by infrequent (but not negligible) low SNR signals. If the turbulence intensities computed in the two data samples agreed within the limits of the statistical uncertainty, as they must in the absence of spurious measurements,† both sets were accepted as valid data. If not, only the second sample was accepted.

All the results presented in Sec. III were based on a minimum of 300 data points for each measurement station and beam orientation; however, 600 measurements was more typical. No corrections were made for the "Doppler ambiguity" in the turbulence intensity determinations since in single-particle, time-domain signal processing the measurements are insensitive to it.[9] Also, no adjustments were made for noise-in-signal effects on the rms measurements.

† In the case of a gaussian-distributed random variable for which the instantaneous velocity approaches,[8] the error in $\langle V' \rangle$ caused by ignoring points outside three standard deviations of the mean is only -1.4%, well below the statistical uncertainty of a 100-point sample size ($\simeq \pm 5\%$ in $\langle V' \rangle$ assuming a 50% confidence interval).

Only the naturally occurring particles in the flow were used for light scattering. The tunnel air was quite clean as compared to ambient air, which is believed to be a consequence of the supply air being dried to a specific humidity never exceeding 0.0001. The maximum particle crossing rate as determined by triggering an oscilloscope on the single-particle bursts and then counting the number of oscilloscope triggers per unit time was only $\simeq 200$/sec. This was surprisingly low considering that the flow was traveling at 600 m/sec. To gain some insight into the size of the naturally occurring particles, tobacco smoke (for which the particle size is fairly well established[10]; 0.16-μm-diam at maximum population, 0.54-μm-diam maximum size) was injected into the tunnel plenum chamber. The scattered light levels produced by the tobacco smoke were essentially the same as those for the naturally occurring particles which implied similar sizes.

Given the particle size, the particle specific gravity, and the local flow conditions, the response of that particle to sinusoidal fluctuations in velocity of the surrounding fluid can be estimated.[11] The analysis, which assumes the viscous drag to be represented by Stokes drag with the Cunningham correction, gives the particle response to turbulence fluctuations as seen relative to the particle's moving frame of reference. The frequency at which the particle response is 3 db down is given by the expression

$$f_{3db} = \frac{1}{2\pi} \frac{18\mu}{\rho_p d_p^2 (1 + kl/d_p)}$$

For the flow conditions of the present study and assuming a particle specific gravity of unity, this frequency is approximately 60 kHz and 120 kHz for a 0.5-μm and 0.3-μm-diam particle, respectively.

Unfortunately, it is difficult to relate these frequencies to their equivalent counterpart in a fixed frame of reference. A relationship can be obtained if the assumption is made that the turbulent fluctuations relative to the moving particle are approximately the same as would be observed in a frame of reference moving at the local mean velocity. In this latter case, turbulent eddies connected at the velocity, u_c, are observed to have the velocity $u_c - \bar{u}$. Whereas in a fixed frame of reference, they are observed to be traveling at u_c. The turbulent frequencies in the two cases are thus related by the velocity ratio $u_c/|u_c - \bar{u}|$ which has been found to be 4 or greater in a compressible turbulent boundary layer.[12] Based on this argument, the frequencies previously given correspond to frequencies of at least 240 kHz and 480 kHz in a fixed frame of reference.

III. Results

The streamwise mean velocity and turbulence intensity were obtained with the incident laser beams orientated so that only the streamwise velocity component was sensed. Figure 2 shows a comparison of the laser velocimeter mean data with the pitot-tube measurements of Ref. 4 which were reduced on the assumption of constant static pressure and total temperature across the boundary layer.

The agreement in mean velocity (see figure insert) is quite good, especially in the freestream (within 0.5%). The largest differences were recorded near the wall ($y \leqq 0.4$ cm); however, these differences can easily be attributed to pitot-tube displacement effects[13] and positioning errors. Neither explains the near constant difference of 2% in the two measurement techniques through the major portion of the boundary layer. Particle slippage, if existent, would result in low laser velocimeter velocity readings since the flow, in general, is from the inner to the outer region of the boundary layer. However, another plausible explanation is inaccuracies in the pitot-tube readings due to turbulence fluctuations, the asymmetry of these fluctuations, and the assumption of constant static pressure across the boundary layer. Measurements were taken with the laser velocimeter at $y = 1$ cm with a $2\langle V' \rangle$ condition employed rather than $3\langle V' \rangle$. Interestingly, the mean velocity computed in this case was within 0.5% of the pitot-tube data which is an indication of the asymmetry in the velocity fluctuations.

The turbulence intensity results are given in Fig. 3. Included in this figure are the incompressible measurements of Klebanoff[8] and the compressible results of Rose[14] and Kistler[15] all of which were obtained by hot-wire anemometry. The freestream velocity was chosen for nondimensionalizing the velocity fluctuations

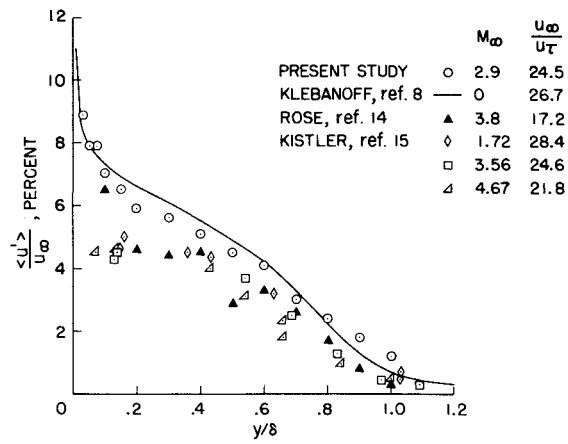

Fig. 3 Streamwise turbulence intensity in a turbulent boundary layer.

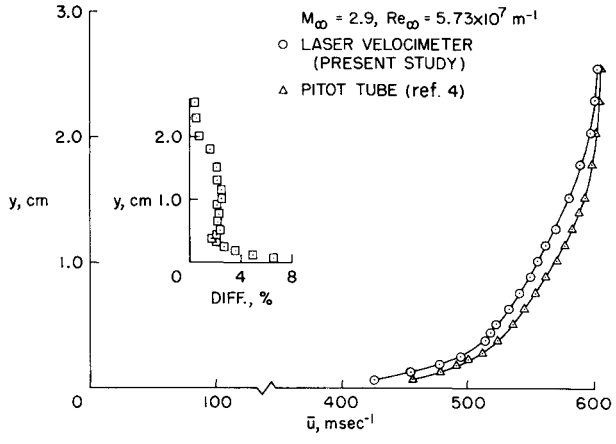

Fig. 2 Laser velocimeter and pitot-tube mean velocity measurements of a supersonic boundary layer.

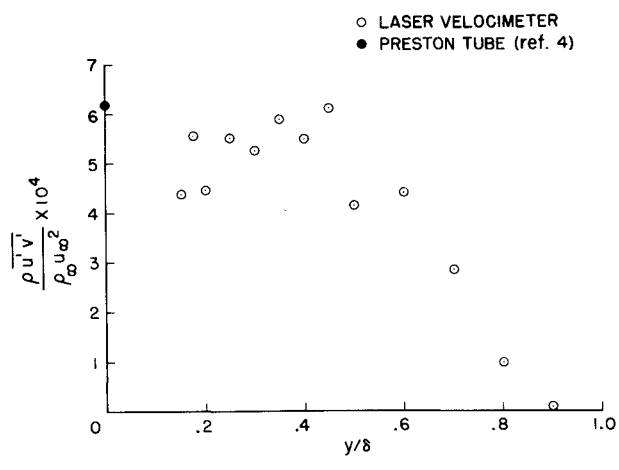

Fig. 4 Reynolds stress distribution for a supersonic boundary layer.

since it appeared to best collapse the data. For the different sets of measurements, the ratio u_∞/u_τ is given to indicate what differences scaling by u_τ would have. As shown by Fig. 3, the results of the present study are strikingly similar to the incompressible results of Klebanoff. The turbulence intensity was not observed to level off in the inner part of the boundary layer as did Kistler's measurements.

Plotted in Fig. 4 are the Reynolds stress, $\rho u'v'$, results in an appropriately nondimensionalized form (the density ratio, ρ/ρ_∞ was calculated from pitot-tube data, assuming constant total temperature) and the wall shear stress as determined from Preston tube data. Apparent from this figure is the general agreement in the Reynolds shear stress in the inner portion of the boundary layer and the wall shear stress as would be expected for a zero pressure gradient boundary layer. The scatter in the Reynolds stress measurements can be attributed to the combined effect of a limited number of data samples and the differencing of two relatively large numbers. Values of $\overline{u'v'}$ for y/δ less than 0.15 are not reported since the lower frequency cutoff of the AEDC processing unit prevented the acceptance of all data within $3\langle V'\rangle$ of the mean at these locations.

IV. Conclusions

In this Note, measurements taken in a Mach 2.9 turbulent boundary layer are presented that demonstrate the ability of the laser velocimeter to measure the turbulence transport properties of high-speed compressible flows. This demonstrated ability combined with the nonperturbing quality and relative insensitivity to environmental conditions of the laser velocimeter open the way to compressible flow measurements never considered possible with more conventional measurement techniques.

References

[1] Van Driest, E. R., "Turbulent Boundary Layer in Compressible Fluids," *Journal of the Aeronautical Sciences*, Vol. 18, No. 3, March 1951, pp. 145–160.

[2] Morkovin, M. V., "Effects of Compressibility on Turbulent Flows," *The Mechanics of Turbulence*, Gordon and Breach, New York, 1964, pp. 367–380.

[3] Laufer, J., *Thoughts on Compressible Turbulent Boundary Layers*, NASA SP-216, Dec. 1968.

[4] Reda, R. C. and Murphy, J. D., "Shock Wave/Turbulent Boundary-Layer Interactions in Rectangular Channels," *AIAA Journal*, Vol. 11, No. 2, Feb. 1973, pp. 139–140.

[5] Logan, S. E., "A Laser Velocimeter for Reynolds Stress and Other Turbulence Measurements," *AIAA Journal*, Vol. 10, No. 7, July 1972, pp. 933–935.

[6] Yanta, W. J. and Smith, R. A., "Measurements of Turbulence-Transport Properties with a Laser Doppler Velocimeter," AIAA Paper 73-169, Washington, D.C., 1973.

[7] Lennert, A. E., Hornkohl, J. O., and Kalb, H. T., "Applications of Laser Velocimeters for Flow Measurements," *Proceedings of the Air Breathing Propulsion Conference*, Monterey, Calif., Sept. 1972.

[8] Klebanoff, D. S., "Characteristics of Turbulence in a Boundary Layer with Zero Pressure Gradient," Rept. 1247, 1955, NACA.

[9] Johnson, D. A., "Insensitivity of Single Particle Time Domain Measurements to Laser Velocimeter 'Doppler Ambiguity'," *AIAA Journal*, Vol. 11, No. 6, June 1973, pp. 890–892.

[10] Green, H. L. and Lane, W. R., *Particulate Clouds: Dusts, Smokes and Mists*, Van Nostrand, Princeton, N.J., 1964.

[11] Yanta, W. J. and Gates, D. F., "The Use of a Laser Doppler Velocimeter in Supersonic Flow," AIAA Paper 71-287, Albuquerque, N.Mex., 1971.

[12] Owen, F. K. and Horstman, C. C., "On the Structure of Hypersonic Turbulent Boundary Layers," *Journal of Fluid Mechanics*, Vol. 53, Pt. 4, 1972, pp. 611–636.

[13] Allen, J. M., "Pitot-Probe Displacement in a Supersonic Turbulent Boundary Layer," TN D-6759, 1972, NASA.

[14] Rose, W. C., "Turbulence Measurements in a Compressible Boundary Layer Subjected to a Shock-Wave-Induced Adverse Pressure Gradient," AIAA Paper 73-167, Washington, D.C., 1973.

[15] Kistler, A. L., "Fluctuation Measurements in a Supersonic Boundary Layer," *Physics of Fluids*, Vol. 2, No. 3, May–June 1959, pp. 290–296.

Shell Instability Analysis Applied to a Radome

TERRY L. JANSSEN* AND THOMAS G. SWANEY†

The Boeing Company, Wichita, Kansas

Introduction

In the instability analysis of shells, a bifurcation buckling analysis is the easiest and least expensive. A bifurcation point defines a load level at and above which some new deformation mode is possible. The bifurcation buckling analysis is based on the classical approach of solving a linear eigenvalue problem. The lowest eigenvalue, denoted as the classical buckling load, represents a prestressed state at which another equilibrium state is possible. The uncertainty of the classical buckling load for arbitrary shells is well known.[1,2] It is clear from experimental results that more than the knowledge of the classical buckling load and its corresponding mode shape is required to yield the load at which an arbitrary shell will collapse. For a general shell, if the shell geometry deteriorates appreciably or stresses are redistributed in the subcritical load range, failure usually occurs by means of collapse at a limit point rather than through bifurcation.

Theory

In the theory of elasticity, geometric nonlinearity is introduced from two sources: the strain-displacement equations and the equilibrium equations. In the finite element technique, the nonlinear strain-displacement relationships are recognized through the use of the differential stiffness matrix, also called the geometric or initial stress stiffness matrix. This matrix is added to the linear stiffness matrix and is a function of the elemental internal loads. The nonlinear equilibrium equations are recognized by using an incremental step procedure. The actual deformed geometry is taken into account at the start of each step.

To demonstrate the manner in which the finite element method satisfies the nonlinear strain-displacement relationships it is convenient to separate the strain energy into two parts

$$U = U_L + U_{NL} \tag{1}$$

U_L is due to the linear strain displacement terms. U_{NL} is due to the nonlinear terms caused by rotation of the element. The

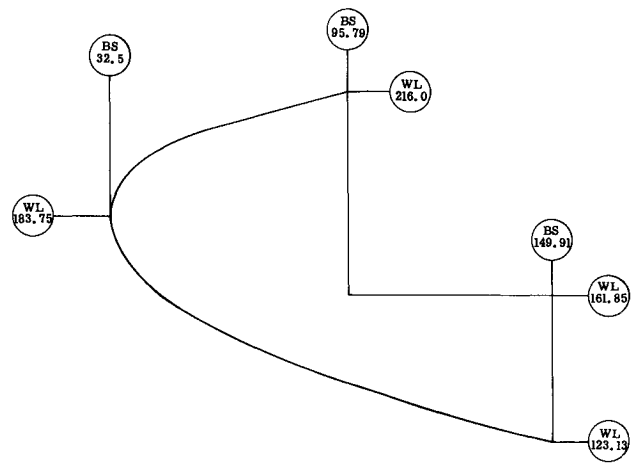

Fig. 1 Structural side view.

Received August 2, 1973.

Index categories: Aircraft Structural Design (Including Loads); Structural Stability Analysis; Structural Static Analysis.

* Senior Engineer, Structures Staff.

† Senior Group Engineer, Structures Staff.